

The SDSU Broadband Ground Motion Generation Module BBtoolbox Version 1.5

Kim Olsen* and Rumi Takedatsu

Dept. of Geological Sciences

GMCS 231A

San Diego State University

5500 Campanile Dr

San Diego, CA 92182, USA

kbolsen@mail.sdsu.edu

* corresponding author.

This manuscript has an electronic supplement that contains descriptions of the validation events and scenarios and fixed and region-dependent parameters, additional goodness-of-fit plots for GMPEs versus data, simulations versus GMPEs, and PSA bias versus distance, and comparison of rupture models with associated PSA bias and time histories for Landers.

Introduction

The Southern California Earthquake Center (SCEC) has completed Phase 1 of its Broadband Platform (BBP) ground motion simulation results, evaluating the potential applications for engineering of the resulting 0.01-10 s Pseudo-Spectral Accelerations (PSAs) generated by 5 different methods. The exercise included part A, where the methods were evaluated based on the bias of simulation results to observations for 12 well-recorded historical earthquakes: 7 in western U.S., 2 in Japan, and 3 in eastern US/Canada. In addition, part B evaluated simulation results for M_w 5.5, M_w 6.2 and M_w 6.6 scenarios at 20 km and 50 km from the fault. The methods were assessed based on the bias of the median PSA for the 12 events in part A, and on a specified acceptance criterion compared to NGA-West Ground Motion Prediction Equations (GMPEs) in part B. The results were evaluated by the bias of mean PSA from simulations using 1D velocity models with $V_s^{\min}=863$ m/s (see electronic supplement of Goulet et al., this issue) with respect to recorded data corrected for site effects. The part A events and part B scenarios are described in Tables S1 and S2, respectively, in the electronic supplement to this article.

One of the 5 methods evaluated was the Broadband Synthetics Generator Module BBtoolbox, a hybrid method combining deterministic low-frequency (LF) synthetics with high-frequency (HF) scatterograms (Mai et al., 2010, Mena et al., 2010). The LFs may be computed using deterministic or dynamic descriptions in 1D or 3D media. The HF scatterograms are generated for each component of motion based on the theory for multiple S-to-S scattering by Zeng et al. (1991, 1993). The scatterograms are based on

user-specified site-scattering parameters and are partly based on the site-specific velocity structure. The seismic scattering wave energy is realized to appear after the direct P wave arrival time, which is found from 3D ray tracing (Hole, 1992). Finally, the scatterograms are convolved with an appropriate source-time function. It is assumed that the scattering operators and moment release originate throughout the fault, but starts at the hypocenter. The hybrid broadband seismograms are calculated in the frequency domain using a simultaneous amplitude and phase matching algorithm (Mai and Beroza, 2003). In the validation exercise, the LFs are generated using 50 source realizations from the kinematic source generator module by Graves and Pitarka (2014) on the SCEC BBP, through the Standard Rupture Format (SRF), identical to those used by the Graves and Pitarka method.

BBtoolbox V1.4 (as described in Mai et al., 2010; Mena et al., 2010) merges LFs and HFs by adjusting the level of the HF acceleration spectra to the corresponding LF spectral value at a specified merging frequency. This procedure was introduced in part to ensure continuity in the broadband synthetics at the merging frequency. While this approach tends to work well for LFs calculated in well-constrained 3D structural models, the results for simplified 1D velocity models averaged over a region was found to generate, at times, strongly biased HF PSA levels. In addition, the scaling of the HFs to the LFs carries any directivity effects from the LFs to arbitrarily high frequencies, also not supported by data. In addition, the shape of the existing source time functions often times did not capture the shape of the PSA trends. The bias introduced by these issues did not permit BBtoolbox V1.4 to pass the SCEC validation phase 1.

In order to obtain more accurate broadband synthetics, as defined by the SCEC validation phase 1 targets and respective 1D Green's Functions (GFs), we generated BBtoolbox V1.5. This article describes the changes that were made to BBtoolbox V1.4 to obtain V1.5, and presents the improved results that enabled BBtoolbox V1.5 to pass the validation.

BBtoolbox V1.5

BBtoolbox V1.5 contains two significant changes, as compared to V1.4. The first modification relates to the merging procedure, where BBtoolbox V1.5 scales (or 'anchors') the HF's to a theoretical spectral level, rather than the level of the LF's. The merging procedure for V1.5 involves the computation of a single spectral scaling value for each station since the merge between LF's and HF's is performed in the frequency domain. This scaling value is in part based on Graves and Pitarka (2010), with many similarities and some differences that are described below.

Graves and Pitarka (2010) calculate the spectral acceleration amplitude as

$$A_i(f) = C_{ij} S_i(f) G_{ij}(f) P(f), \quad (1)$$

where $C_{ij} = F_s R_{p_{ij}} / [4\pi\rho_i\beta_i^3]$ is a radiation scale factor, with $F_s = 2$ accounting for the free surface amplification, $R_{p_{ij}}$ is a conically averaged (P and S-wave) radiation pattern term from the take-off angle and focal mechanism, and ρ_i and β_i are density and shear-wave velocity in the middle of each subfault.

$$S_i(f) = m_i (M_o/N) (2\pi*f)^2 [1 + F(f/f_{ci})^2]^{-1} \quad (2)$$

is a source radiation term, where $m_i = d_i \mu_i A_T / M_0$ is the average subfault moment calculated using the slip (d_i) and shear modulus (μ_i) of the i th subfault as well as the total fault area A_T . $F = M_0 / [N \text{ strfac } dl^3]$ is a scaling factor for the subfaults where M_0 is the total scalar moment, N is the number of subfaults, strfac is the Brune stress parameter, and dl is average subfault dimension. $f_{ci} = c_0 V_{Ri} / [\alpha_T \pi dl]$ and V_{Ri} are the corner frequency and rupture velocity, respectively, of the i th subfault, and α_T is a scale factor accounting for the fault dip (δ)-dependence of the ground motion. α_T is calculated as

$$\alpha_T = 0.82 \text{ for } \delta \leq 55^\circ \text{ and } 1 \text{ for } \delta \geq 70^\circ \quad (3)$$

with a linear transition between dips of 55° and 70° . Note that this calculation of α_T is slightly different from that of Graves and Pitarka (2010), based on comparisons of selected BBtoolbox V1.5 synthetics with those from GMPEs; also note the typos in Graves and Pitarka (2010, Eq. 12).

Graves and Pitarka calculate the path effect term $G_{ij}(f)$ of the j th ray from the i th subfault to the station as

$$G_{ij}(f) = I_i(f) \exp(-\pi f^{1-f_{dec}} T/Q_0) / r_{ij}(x), \quad (4)$$

where $I_i(f)$ is the impedance effect from the quarter-wavelength theory outlined by Boore and Joyner (1997), and $r_{ij}(x)$ is the total path length of the j th ray from the i th subfault to the receiver. $Q(f)$ is approximated as a power law $Q_0 f^{f_{dec}}$, and T/Q_0 is approximated as $\sum t_{ijk} / q_k$, where t_{ijk} is the travel time of the j th ray from the i th subfault to the station, $q_k = a_{fac} + b_{fac} \beta_k$, where a_{fac} and b_{fac} are regionally-dependent empirical constants and β_k is the shear-wave velocity of the k th layer, and the sum is over the stack of layers in the 1D crustal model.

At low frequencies, the acceleration spectra of the subfaults $A_i(f)$ in Eq. 1 sum coherently to the total spectrum as $A(f)=N \Sigma A_i(f)$, where N is the sum of the subfaults. However, as shown by Joyner and Boore (1986) this summation becomes frequency dependent due to destructive interference of random phasing. More specifically, at the high frequency limit, we get

$$A(f)=(N^{1/2}/N) \Sigma A_i(f). \quad (5)$$

While the HF amplitudes for Graves and Pitarka vary with frequency, we define a scaling of the HFs for BBtoolbox V1.5 based on Eqs. 1-4 that applies to all frequencies larger than the merging frequency for a given source-station pair. This scaling value is calculated using $f=50\text{Hz}$ in Eqs. 1-2, a frequency sufficiently high to honor the criterion in Eq. 5. However, due to the scaling of the HFs by a single average value, we use an additional average multiplicative factor of 1.4 in Eq. 5 to obtain an optimal performance as measured by the part A and B scenarios. BBtoolbox V1.5 uses $f=1\text{Hz}$ in Eq. 4, and incorporates $Q=Q_0 f^{f_{\text{dec}}}$ into the scatterograms for all frequencies above the merging frequency. We extract fault and rupture parameters used to calculate the scaling directly from the kinematic source description generated in standard rupture format (srf) from the Graves and Pitarka rupture generator implemented on the BBP. Finally, BBtoolbox V1.5 uses a magnitude-dependent merging frequency, 1 Hz for $M_w \geq 5.25$ and 2 Hz for $M_w \leq 4.75$, with a linear transition of the merging frequency between M_w 4.75 and 5.25.

We approximate the distance between subfaults and receivers in Eq. 4, $r_{ij}(x)$ as a straight path for source-station distances ≤ 200 km, which is the range used for most scenarios in the validation. However, for source-receiver distances beyond 200 km,

which was considered for the eastern scenario Mineral (up to 300 km) due to a sparse data set, a revised distance term of $r_{ij}^{1.1}(x)$ was used to obtain an acceptable fit to data. This increases the source-station distance for long-range wave propagation which may be explained by the development of multiply-reflected ray paths inside the crust. Further tests are needed to examine this issue, and whether it is specific to eastern North America events.

The other change to BBtoolbox V1.4 to obtain V1.5 is the shape of the source time function used for convolution with the scattering GFs. Mai et al. (2010) and Mena et al. (2010) used BBtoolbox srcV1.4 with the source time function defined by Dreger et al. (2007). However, a different source time function has been implemented in V1.5 with its rise-time scaled as a function of M_w , which provides a better fit of PSA curves between synthetics and data, and has been used exclusively for all scenarios in the validation. The functional form of this source-time function is

$$S(t)=t^{0.5} / [1+(t/t_0)^2], \quad (6)$$

where $t_0=T_{\text{rfac}}*T_r$, $T_r=\alpha_T 2.03*M_0^{1/3}/10^9$ with M_0 in dyne cm (see Fig. 1), and T_{rfac} is a M_w -dependent rise time scaling factor given by

$$T_{\text{rfac}}= 0.141-0.09 \tan^{-1}(1.6 M_w -9.55) \quad (7)$$

and α_T is given in Eq. 3 (see Fig. 2). Since T_{rfac} scales the ground motion amplitudes as well as appears strongly dependent on earthquake size, these relations should be used with caution outside the range tested here (M_w 4.6-7.2).

Results

BBtoolbox V1.5 was validated on the BBP for the SCEC validation Phase 1. The parameters used (fixed and region-specific) are listed in Tables S3 and S4, respectively, in the electronic supplement to this article. Figure 3 shows bias of the Pseudo Spectral Acceleration (PSA) for an ensemble of 50 realizations for the 7 western U.S. and 2 Japan events. In general, the fits are good, except the relatively large overprediction for Alum Rock for most periods. This bias is likely due to a large negative event term (average data residuals), supported by similar overprediction by leading GMPEs (see Fig. S1 in the electronic supplement to this article). The fits are generally best for shorter periods ($<1s$), as there is some tendency to overpredict for the longer periods ($>1s$). The bias for the eastern U.S./Canadian events are shown in Figure 4. The overall best fits for a constant stress parameter (strfac in Eq. 2) are obtained for 350 bars (Fig. 4, left). However, a slightly improved fit (for Mineral and Saguenay) is obtained assuming a depth-dependent value of the stress-parameter of the following form

$$\text{strfac} = 6.25 Z_{\text{tor}} + 265 \text{ bars} \quad (8)$$

generating values of strfac of 302 bars for Mineral, 342 for Riviere du Loup, and 399 bars for Saguenay (see Fig. 4, right). Here, Z_{tor} is the depth to the top of the rupture. While some evidence of a depth-dependent stress parameter for eastern North America has been found (Boatwright and MacDonald, 2012), such trend is still uncertain. Table S1 provides goodness-of-fit values binned for various period and distance ranges as well as mechanism for the part A validation results generated by BBtoolbox V1.5.

The performance of the SDSU module for part B of the validation is shown in Figure 5 for northern California 1D velocity model (see Fig. S2 in the electronic

supplement to this article for results using the southern California 1D model). Here, PSAs (0.01-10s) for M_w 5.5, 6.2, and 6.6 scenarios are compared for simulations and leading GMPEs (see Goulet and Abrahamson, 2014, for definition of the acceptance criteria). The mean PSAs from the simulations obtained by the SDSU module show very good agreement with the GMPEs and fall within the applicable acceptance criteria for all scenarios periods.

The validation results for the SDSU module were checked for bias from various parameters in the modeling. Figs. S3-S15 in the electronic supplement to this article show bias versus fault-station distance for the part A events. In addition, Table 1 lists goodness-of-fit (GOF) values binned by distance, PSA period and event mechanism. The GOF values for BBtoolbox V1.5 generally fall within the green (considered passing the validation) and white entries (marginal acceptance) for PSA periods < 1 s and all mechanisms, but tend to increase for longer periods. The table and plots indicate no obvious bias with respect to fault-station distance, PSA period, fault mechanism, dip, and magnitude. It is also encouraging to notice that the rupture and slip pattern for the source realizations generating the best fits appear in general better agreement with the kinematic inversion models (see, e.g., Figure S16 in the electronic supplement to this article). Moreover, the computed broadband synthetics appear realistic (see, e.g., Figure S17 of the electronic supplement to this article).

Summary and Future Work

The SDSU broadband Ground Motion Generation Module BBtoolbox V1.5 was obtained from modifications to BBtoolbox V1.4 (Mai et al., 2010; Mena et al., 2010).

The most significant modification is the ‘anchoring’ of the HF spectral acceleration of the broadband time series to the LF component using a theoretical level calculated from the finite fault source description and path effects. In addition, we have introduced a new source time function for convolution with the HF scattering functions, and a modified geometrical spreading factor for long-range wave propagation (at least for eastern US/Canadian events).

Due to these modifications, BBtoolbox V1.5 passed the SCEC BBP Phase 1 validation. No significant bias of the median PSA (0.01-10s) with respect to distance, magnitude, fault mechanism, depth to the top of the fault, or PSA period was observed for the method using 7 events in the western U.S., 2 Japanese events, and 3 eastern U.S./Canadian events, and the synthetic time histories appear realistic. Moreover, mean PSAs computed by BBtoolbox V1.5 were all within the acceptance level for all distances and PSA periods for four M_w 5.5-6.6 scenarios with respect to leading NGA-West GMPEs.

The long-period results for the SDSU (and thus for the Graves and Pitarka method) synthetics were found to overpredict the strong motion data and GMPEs in several cases (see Figs. 3-5). While the reason for this long-period trend has not been determined, possible explanations include the use of simplified 1D crustal GFs for the simulations that may be generating too coherent wave trains, source descriptions (including magnitude-fault area relation and rupture complexity), and the omission of near-fault plastic (nonlinear) effects, as pointed out by Roten et al. (2014).

Based on the performance in the validation exercise we expect BBtoolbox V1.5 to work satisfactorily for forward simulation of earthquake scenarios with magnitudes between 4.5 and 7.22 for all PSA periods and source-station distances up to at least 200 km. However, it should be cautioned that the accuracy of the long-period (>1 s) PSAs depend on the performance of the rupture generator and the 1D GFs, and that larger magnitude events need further validation. We find that using magnitudes specified in NGA-West2 for historical earthquakes and the definition of the fault area based on earthquake magnitude by Leonard (2010) are appropriate for the use of BBtoolbox V1.5. However, we caution that the aspect ratio of the fault should be chosen not to violate any available constraints on the seismogenic depth.

On-going and future efforts related to BBtoolbox V1.5 will include validations for magnitudes larger than those tested here (e.g., $M_w 7.22$), PSA variability for multiple realizations on a single event, and further calibration of the depth-dependent stress parameter scaling for eastern U.S./Canadian events. Future development of the code will consider Fourier spectra in addition to PSA metrics.

Acknowledgements. We are grateful for the comments from Jack Baker and an anonymous reviewer. This work was supported by SCEC, which is funded by NSF Cooperative Agreement EAR-0529922 and USGS Cooperative Agreement 07HQAG0008, as well as NSF Award OCI-1148493 (SI2-SSI). We acknowledge the Pacific Earthquake Engineering Research (PEER) center for providing the recorded data.

References

Abrahamson, N. A., and W. J. Silva (2008). Summary of the Abrahamson & Silva NGA Ground-Motion Relations, *Earthquake Spectra*, 24(1), 67-97.

Boatwright, J., and T. MacDonald (2012). The Variation of Brune Stress Drop with Hypocentral Depth for Moderate ($2.5 \leq M \leq 5.8$) Earthquakes in Northeastern North America, Abstract presented at the Annual Meeting of the Eastern Section of SSA, Blacksburg, VA, Oct 28-30, 2012.

Boore, D.M., and G.M. Atkinson (2008). Ground-motion prediction equations for the average horizontal component of PGA, PGV, and 5%-damped PSA at spectral periods between 0.01 and 10.0 s, *Earthquake Spectra* 24, No. 1, pages 99-138.

Campbell, K. W. and Y. Bozorgnia (2008). NGA ground motion model for the geometric mean horizontal component of PGA, PGV, PGD and 5% damped linear elastic response spectra for periods ranging from 0.01 to 10s, *Earthquake Spectra*, 24(1), 139-171.

Chiou, B. S.-J. and Youngs R. R. (2008). An NGA model for the average horizontal component of peak ground motion and response spectra, *Earthquake Spectra*, 24(1), 173-215

Dreger, D., E. Tinti, and A. Cirella (2005). Slip velocity function parameterization for broadband ground motion simulation, *Seismol. Soc. Am 2007 Annual Mtg*, Waikoloa, Hawaii, 11-13 April 2007.

Goulet, C.A., and N.A. Abrahamson (2014). The SCEC Broadband Platform validation exercise: methodology for code validation in the context of seismic hazard analyses, *Seism. Res. Lett.*, this issue.

- Graves, R.W., and A. Pitarka (2010). Broadband ground-motion simulation using a hybrid approach, *Bull. Seis. Soc. Am.* **100**, 5A, 2095-2123, doi: 10.1785/0120100057.
- Graves, R.W., and A. Pitarka (2014). Refinements to the Graves and Pitarka (2010) Broadband Ground Motion Simulation Method, *Seism. Res. Lett.*, this issue.
- Hole, J.A. (1992). Non-linear high resolution three-dimensional seism travel time tomography, *J. Geophys. Res.* **97**, 6553-6562.
- Joyner, W.B., and D.M. Boore (1986). On simulating large earthquakes by Green's function addition of smaller earthquakes, in *Earthquake Source Mechanics, Geophysical Monograph 37*, Maurice Ewing Vol. 6, Eds S. Das, J. Boatwright, and C.H. Scholz.
- Leonard, M. (2010) Earthquake fault scaling: self-consistent relating of rupture length, width, average displacement, and moment release, *Bull. Seis. Soc. Am.* **100**, 5A, 1971-1988.
- Mai, P.M. and G.C Beroza (2003). A hybrid method for calculating near-source, broadband seismograms: Application to strong motion prediction, *Phys. Earth Planet. In.* **137**, no 1-4, 183-199.
- Mai, P.M., W. Imperatori and K.B. Olsen (2010). Hybrid broadband ground-motion simulations: combining long-period deterministic synthetics with high-frequency multiple S-to-S backscattering, *Bull. Seis. Soc. Am.* **100**, 5A, 2124-2142, doi: 10.1785/0120080194.

Mena, B., P.M. Mai, K.B. Olsen, M.D. Purvance, and J.N. Brune (2010). Hybrid broadband ground-motion simulation using scattering Green's functions: application to large-magnitude events, *Bull. Seis. Soc. Am.* **100**, 5A, 2143-2162, doi: 10.1785/0120080318.

Roten, D., K.B. Olsen, S.M. Day, Y. Cui, and D. Fah (2014). Expected seismic shaking in Los Angeles reduced by San Andreas fault zone plasticity, *Geophysical Research Letters*, doi:10.1002/2014GL059411 (available online 12 April 2014).

Zeng, Y.H., K. Aki, and T.L. Teng (1993). Mapping of the high-frequency source radiation for the Loma Prieta earthquake, California, *J. Geophys. Res.* **98**, no. B7, 11981-11993.

Zeng, Y.H. F. Su, and K. Aki (1991). Scattering wave energy propagation in a random isotropic scattering medium 1. Theory, *J. Geophys. Res.* **96**, no. B1, 607-619.

Figure Captions.

Figure 1. Shape of the source-time function convolved with the scatterograms in BBtoolbox V1.5.

Figure 2. M_w -dependent scaling factor for the rise time used for the source time function (see Fig. 1).

Figure 3. Combined (50 realization) PSA bias ($\ln[\text{data}/\text{model}]$) for the 7 western US and 2 Japan events. Thick line depicts the median, dark shading shows the 95% confidence interval, and light shading is for the standard deviation.

Figure 4. Combined (50 realization) PSA bias for the 3 eastern US/Canadian events. Results for stress parameter strfac (left) fixed at 350 bars and (right) depth-dependent.

Figure 5. Part B of the validation comparing PSAs for 50-realization ensemble synthetics against leading GMPEs for M_w 5.5, 6.2, and 6.6 scenarios. AS08, Abrahamson and Silva, 2008; BA08, Boore and Atkinson, 2008; CB08, Campbell and Bozorgnia, 2008; and CY08, Chiou and Youngs, 2008. The plots show the mean (square) and standard deviation (box), while error bars show extrema for all realizations.

Description of Tables and Figures in the Electronic Supplement to this Article:

Table S1. Description of Part A events. Z_{tor} is depth to the top of the fault.

Table S2. Description of Part B scenarios.

Table S3. Fixed parameters for BBtoolbox V1.5.

Table S4. Region-dependent parameters for BBtoolbox V1.5. Here, c_0 is chosen as 2.1 for active regions, and as 1.1 for stable regions (Somerville et al., 2009).

Figure S1. PSA bias plots for the observed data versus the four GMPEs used in the validation for Alum Rock. AS08 is Abrahamson and Silva, 2008; BA08 is Boore and Atkinson, 2008; CB08 is Campbell and Bozorgnia, 2008; CY08 is Chiou and Youngs, 2008. Note that the GMPEs overpredict the data, similar to but more pronounced than the SDSU synthetics (see Figure 3), suggesting the presence of a relatively large event term for Alum Rock.

Figure S2. Part B of the validation comparing PSAs for 50-realization ensemble synthetics against leading GMPEs for M_w 5.5, 6.2, and 6.6 scenarios, using the southern California 1D velocity model. The plots show the mean (square) and standard deviation (box), while error bars show extrema for all realizations.

Figure S3. PSA bias for selected periods versus distance for the Alum Rock scenario. The dots and error bars depict the median and range of values obtained for the 50 realizations.

Figure S4. Same as Figure S3, but for Chino Hills.

Figure S5. Same as Figure S3, but for Landers.

Figure S6. Same as Figure S3, but for Loma Prieta.

Figure S7. Same as Figure S3, but for North Palm Springs.

Figure S8. Same as Figure S3, but for Northridge.

Figure S9. Same as Figure S3, but for Whittier.

Figure S10. Same as Figure S3, but for Niigata.

Figure S11. Same as Figure S3, but for Tottori.

Figure S12. Same as Figure S3, but for Mineral.

Figure S13. Same as Figure S3, but for Riviere du Loup.

Figure S14. Same as Figure S3, but for Saguenay.

Figure S15. Best fit line (green) and 95% confidence regions (red-dashed) for period bins of 0.01-0.1s, 0.1-1s, 1-3s, and 3-5s including all 12 part A validation events. Y-axis is the mean bias in natural log units. Values are for each distance bin plotted with respect to the natural log of the central distance of each bin. Data are weighted by the number of stations and discrete periods in each distance bin. The ratio is the absolute value of the slope of the trend lines (green) divided by its standard error. Values less than 1 indicate that zero slope lies within the 95% confidence, and constitutes a passing criterion. All SDSU results met this criterion.

Figure S16. (left) Slip and rupture time contours and (right) GOF for the Landers realization with the (top) smallest and (bottom) largest bias. Notice that the rupture and slip pattern for the source generating the best fit appears in general better agreement with the kinematic inversion models obtained for Landers as compared to the source associated with the poorest fit.

Figure S17. (left) map of station locations (circles), fault (black line), and epicenter (star), and (right) Broadband velocity time histories and Arias Intensities for station YER (yellow circle in map) for the Landers realization with the smallest bias (data in black, synthetics in red).

Table 1. Goodness of fit (GOF) summary for SDSU validation results (natural log of observed PSA/predicted PSA) binned by distance, PSA period and event mechanism. Two values are listed for each bin: (left) sum of GOF values, and (right) sum of absolute GOF values. The entries are shaded dark gray ($-0.50 \leq \text{GOF} \leq 0.50$), white ($-0.70 \leq \text{GOF} < -0.50$ or $0.50 < \text{GOF} \leq 0.70$), and light gray ($\text{GOF} < -0.70$ or $\text{GOF} > 0.70$). ROBL, reverse-oblique; SS, strike slip; REV, reverse; CENA, Central Eastern North America. lists the the sum of absolute values is listed to identify over- or underprediction in cases where the sum of the GOF values is small.

	Event (Mw, Mech.)	SDSU 0.01-0.1s		SDSU 0.1-1s		SDSU 1-3s		SDSU >3s	
Rrup=[0-5] km	Chino Hills (5.39, ROBL)								
	Alum Rock (5.45, SS)	-0.65	0.65	-0.78	0.78	-1.32	1.32	-1.05	1.05
	Whittier Narrows (5.89, REV)								
	North Palm Springs (6.12, ROBL)	0.36	0.36	0.22	0.32	-0.51	0.51	-0.95	0.95
	Tottori (6.59, SS)	-0.40	0.40	0.40	0.51	-0.13	0.21	-0.31	0.31
	Niigata (6.65, REV)								
	Northridge (6.73, REV)								
	Loma Prieta (6.94, ROBL)	0.19	0.33	0.29	0.37	-0.12	0.53	-0.39	0.39
	Landers (7.22, SS)	0.92	0.92	0.45	0.45	0.53	0.53	0.44	0.44
	Riviere-du-Loup (4.6 REV)								
	Mineral (5.68 REV)								
	Saguenay (5.81 REV)								
	Average CA	0.20	0.48	0.13	0.44	-0.28	0.66	-0.24	0.54
	Average CENA								
Average ALL	0.11	0.47	0.16	0.45	-0.26	0.60	-0.25	0.49	

Rrup=[5-20] km	Chino Hills (5.39, ROBL)	0.17	0.28	0.29	0.38	0.65	0.65	0.84	0.84
	Alum Rock (5.45, SS)	-0.13	0.25	-0.03	0.38	-0.27	0.60	-0.17	0.68
	Whittier Narrows (5.89, REV)	-0.28	0.43	-0.16	0.40	-0.54	0.55	-1.01	1.01
	North Palm Springs (6.12, ROBL)	-0.11	0.33	-0.17	0.41	-0.30	0.65	-0.05	0.24
	Tottori (6.59, SS)	-0.29	0.32	0.08	0.38	-0.01	0.49	0.04	0.44
	Niigata (6.65, REV)	-0.15	0.52	-0.01	0.44	-0.53	0.81	-0.55	0.68
	Northridge (6.73, REV)	-0.06	0.37	0.16	0.42	-0.14	0.35	-0.10	0.32
	Loma Prieta (6.94, ROBL)	0.18	0.35	0.20	0.39	-0.32	0.40	-0.25	0.28
	Landers (7.22, SS)	-0.29	0.66	-0.02	0.54	-0.36	0.51	-0.85	0.85
	Riviere-du-Loup (4.6 REV)	-0.02	0.35	0.13	1.17	0.57	1.02	1.20	1.20
	Mineral (5.68 REV)	-0.66	0.66	-0.68	0.68	-0.23	0.23	-0.25	0.25
	Saguenay (5.81 REV)								
	Average CA	-0.06	0.37	0.05	0.41	-0.21	0.48	-0.07	0.51
	Average CENA	-0.24	0.45	-0.14	1.01	0.25	0.71	0.84	0.96
Average ALL	-0.09	0.38	0.04	0.43	-0.19	0.52	-0.10	0.53	

Rrup=[20-70] km	Chino Hills (5.39, ROBL)	0.01	0.47	-0.02	0.50	0.10	0.47	0.55	0.63
	Alum Rock (5.45, SS)	-0.72	0.80	-0.70	0.79	-0.81	0.86	-0.55	0.58
	Whittier Narrows (5.89, REV)	-0.27	0.43	-0.25	0.51	-0.51	0.61	-0.49	0.49
	North Palm Springs (6.12, ROBL)	0.30	0.52	-0.01	0.50	-0.15	0.42	-0.43	0.43
	Tottori (6.59, SS)	0.29	0.44	-0.02	0.59	-0.62	0.70	-0.44	0.57
	Niigata (6.65, REV)	0.04	0.43	-0.10	0.55	-0.95	1.07	-1.09	1.13
	Northridge (6.73, REV)	-0.54	0.55	-0.37	0.46	-0.22	0.53	-0.33	0.80
	Loma Prieta (6.94, ROBL)	-0.33	0.43	-0.18	0.42	-0.45	0.57	-0.18	0.36
	Landers (7.22, SS)	-0.27	0.35	-0.27	0.44	-0.55	0.64	-0.73	0.75
	Riviere-du-Loup (4.6 REV)	0.09	0.47	-0.08	0.60	-0.10	0.63	-0.25	0.30
	Mineral (5.68 REV)	-0.16	0.31	-1.18	1.19	-0.05	1.00	-0.07	0.10
	Saguenay (5.81 REV)	0.25	0.35	-1.33	1.33	-1.98	1.98		
	Average CA	-0.25	0.50	-0.26	0.52	-0.38	0.59	-0.35	0.62
	Average CENA	0.08	0.44	-0.34	0.75	-0.11	0.69	-0.23	0.28
Average ALL	-0.15	0.49	-0.23	0.55	-0.45	0.66	-0.54	0.72	

Rrup=[70-300] km	Chino Hills (5.39, ROBL)	0.31	0.55	0.31	0.60	0.19	0.73	0.58	0.91
	Alum Rock (5.45, SS)	-0.54	0.80	-0.48	0.77	-0.85	0.86	-0.86	0.86
	Whittier Narrows (5.89, REV)								
	North Palm Springs (6.12, ROBL)	-0.23	0.26	-0.46	0.50	0.23	0.36		
	Tottori (6.59, SS)	0.36	0.51	0.51	0.67	-0.32	0.70	-0.31	0.58
	Niigata (6.65, REV)	0.22	0.62	0.02	0.63	-1.33	1.36	-1.49	1.50
	Northridge (6.73, REV)	-0.05	0.28	0.19	0.49	-0.32	0.56	-0.31	0.31
	Loma Prieta (6.94, ROBL)	0.54	0.54	0.74	0.77	0.51	0.92	0.03	0.62
	Landers (7.22, SS)	-0.08	0.21	-0.14	0.35	0.03	0.39	0.03	0.47
	Riviere-du-Loup (4.6 REV)	-0.07	0.38	0.04	0.63	0.24	1.00	0.58	0.58
	Mineral (5.68 REV)	-0.03	0.38	0.31	0.51	0.79	0.81	0.20	0.28
	Saguenay (5.81 REV)	0.03	0.38	0.10	0.49	0.50	0.62	-0.13	0.13
	Average CA	-0.01	0.48	0.01	0.57	-0.06	0.65	0.00	0.69
Average CENA	-0.01	0.38	0.15	0.53	0.58	0.77	0.18	0.27	
Average ALL	0.08	0.49	0.12	0.59	-0.22	0.80	-0.52	0.86	
Mechanism	Reverse (REV)	-0.11	0.45	-0.11	0.54	-0.42	0.76	-0.80	0.95
	Reverse-Oblique (ROBL)	0.10	0.45	0.07	0.49	-0.05	0.56	0.16	0.54
	Strike-Slip (SS)	-0.18	0.49	-0.16	0.57	-0.45	0.66	-0.40	0.61
	Normal (NM)								
Total	Average CA	-0.15	0.47	-0.13	0.50	-0.26	0.58	-0.20	0.60
	Average CENA	0.01	0.41	-0.08	0.66	0.28	0.74	0.09	0.33
	Average ALL	-0.07	0.46	-0.08	0.53	-0.33	0.67	-0.44	0.72

Figures

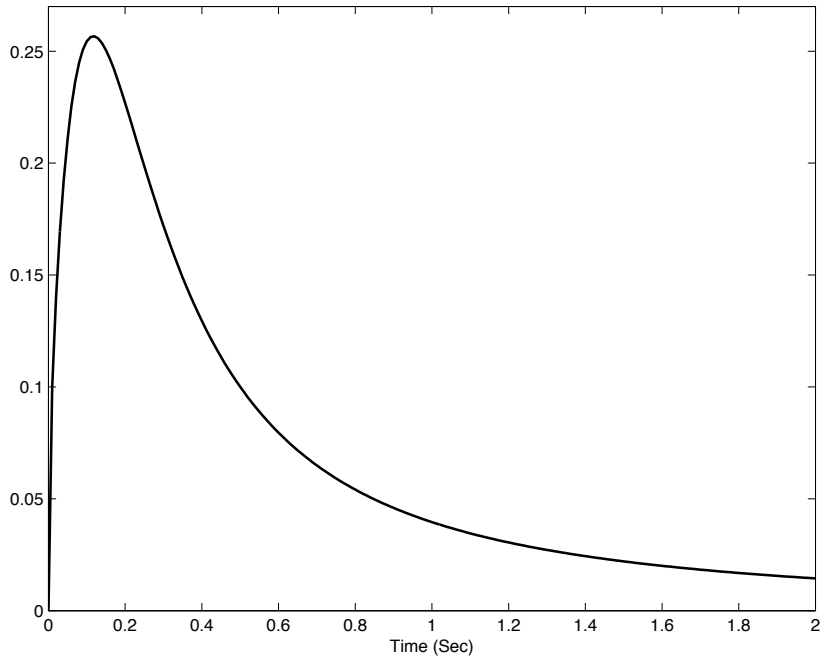


Figure 1.

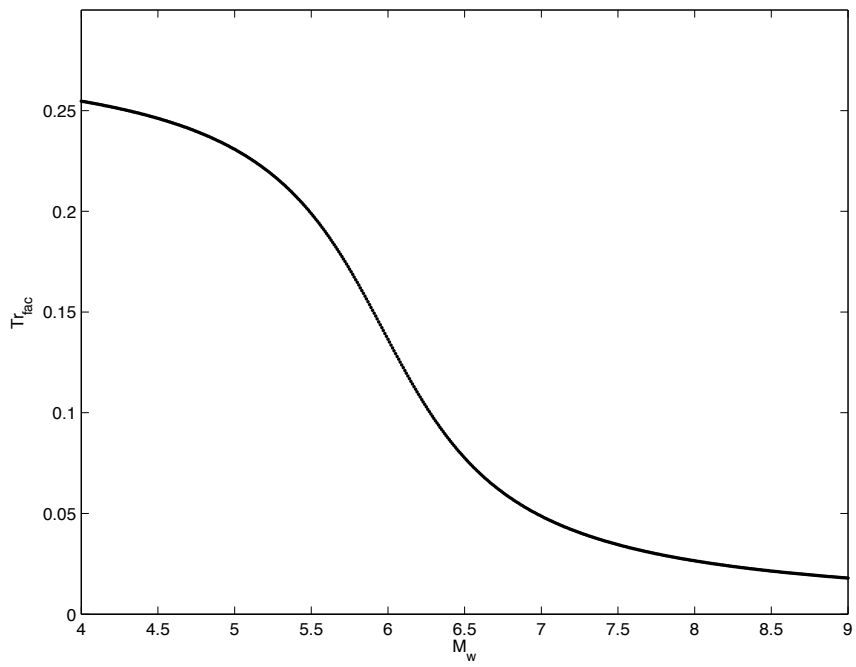


Figure 2.

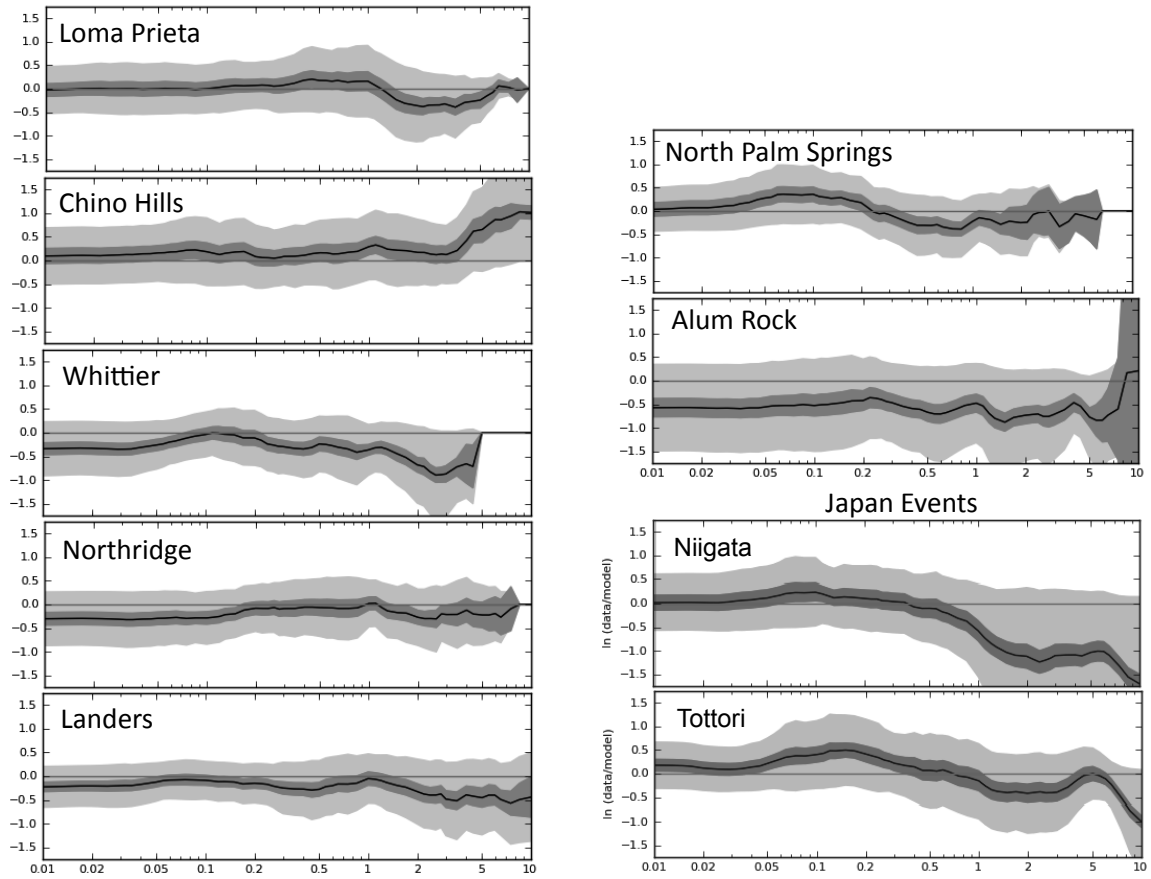


Figure 3.

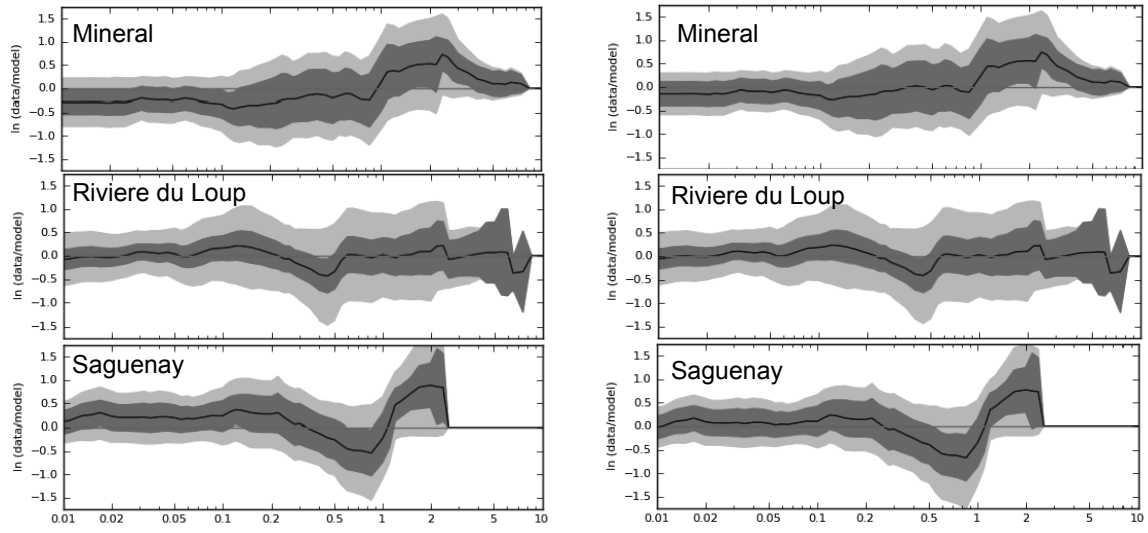


Figure 4.

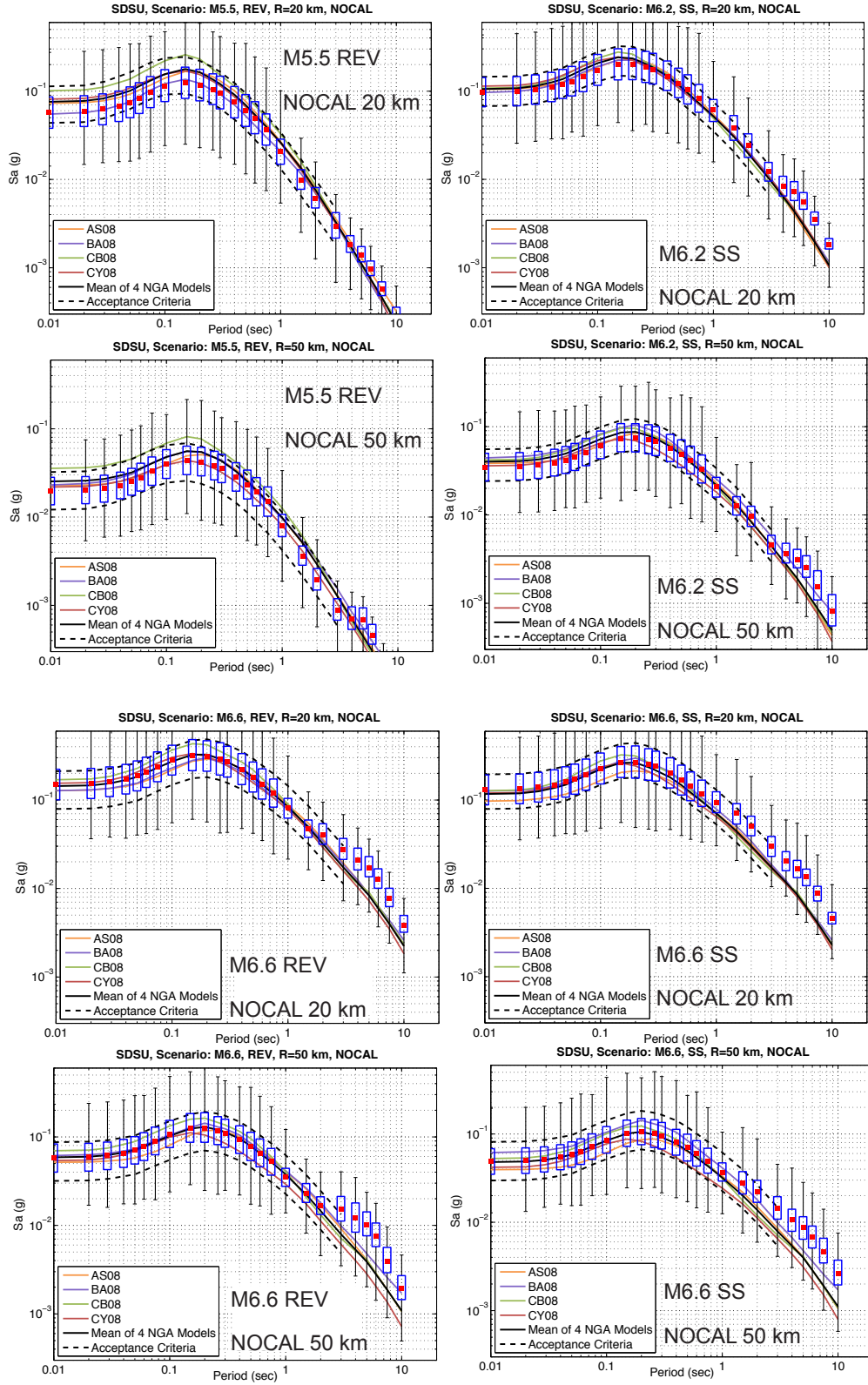


Figure 5.